A Rigorous Graphical Technique for Predicting Sub-harmonic Injection Locking in LC Oscillators

Palak Bhushan
Department of Electrical Engineering and Computer Sciences, The University of California, Berkeley, CA, USA
Email: palak@berkeley.edu

***Abstract*— We develop methods for simply yet rigorously analyzing sub-harmonic injection locking (SHIL) in LC oscillators. Our method respects nonlinearities while offering intuition and design insights into the underlying mechanisms of different modes of locking. It can predict the presence/absence, number, stability and oscillation amplitudes of locks, as well as lock ranges. We use practical LC oscillator topologies from integrated RF and UHF applications for demonstration, validating our technique against SPICE-level simulations while being 1-2 orders of magnitude faster. To our knowledge, this is the first technique/tool for SHIL general enough to treat any kind of nonlinearity in LC oscillators.**

I. Introduction

Injection locking (IL) [1]–[4] is a phenomenon in which an oscillator becomes phase-locked to an external periodic input – called the injection signal – thus oscillating at the same frequency as the input (fundamental harmonic IL or FHIL) or an integral sub-multiple (sub-harmonic IL or SHIL). IL and the related phenomenon of injection pulling [5] are sometimes unwanted (*e.g.*, they can interfere with desired operation in PLLs), but have also found many applications, including for frequency division [6], quadrature signal generation [7], microwave generation in laser optics [8], in analog fibre-optics [9], for speeding lock in PLLs [10], *etc.*. IL is also fundamental in biology, *e.g.*, in circadian rhythms [11], [12].

Sub-harmonic IL, where the oscillator locks to a frequency that is an exact integral sub-multiple of that of the input, has attracted attention for decades [13]–[17]. In recent years, SHIL has found application in RFIC and high-speed digital designs, *e.g.*, for reducing phase noise, clock jitter and PVT sensitivity in VCOs and PLLs [18]–[22]. Virtually all such applications use LC oscillator topologies[1].

There appear to be no effective tools or methods presently available for rapid, insightful or rigorous analysis/design of practical LC oscillator topologies undergoing SHIL. Prior theoretical analyses [15], [16] are limited to specific simplistic nonlinearities/topologies; even for those, they fail to provide useful insight into the SHIL mechanism or into means for its manipulation during design. A theory based on oscillator PPVs [23]–[25] that explores SHIL in generic nonlinear oscillators is available [17], but being abstract, suffers from the same shortcomings.

In this paper, we present a general technique and tool for analysing and understanding SHIL in negative-resistance LC oscillators. Unlike prior work, our technique deals rigorously with arbitrary nonlinearities, while providing direct insight into the SHIL mechanism and its manipulation during design. Limitations of previous methods to simplistic nonlinearities are remedied by incorporating computational components in our procedure. A key feature is that the mathematics involved can be viewed *graphically*, resulting in a procedure that builds intuition and understanding about SHIL. We have implemented this procedure as a tool in **MATLAB**™.

[1]although IL is in fact generic to all nonlinear oscillators [17].

DAC '14, June 01 - 05 2014, San Francisco, CA, USA

http://dx.doi.org/10.1145/2593069.2593076

Our technique represents the physical oscillator as an equivalent signal flow graph that involves a feedback loop with an arbitrary memoryless nonlinearity, an LC filter, and the injection signal. The filtered output of the LC tank combines with the injection signal to excite the nonlinearity with two frequency components, at the injection frequency and a sub-harmonic. The amplitude and phase relationships between these two components are key in determining the output of the nonlinearity, of the many frequency components of which only the one at the sub-harmonic frequency turns out to be important. This frequency-domain I/O characteristic can be pre-characterized computationally, at minimal cost, for any given nonlinearity. The sub-harmonic output of the nonlinearity is filtered by the LC tank, altering its phase and amplitude in a manner that can be expressed analytically (or pre-characterized computationally for complex LC tank topologies). The LC tank's output combines with the injection signal to produce the two-frequency-component input to the nonlinearity, thus completing the loop.

Each step of the above signal flow can be viewed graphically, with intersections between curves representing consistent completions of the feedback loop. This graphical procedure provides direct insight into how lock states change, appear or disappear as the system is manipulated, in a manner that is difficult using non-graphical solution procedures. It also provides a complete picture of the number of locks, their stability, and lock ranges, matching results from PPV-based analysis [17] but providing greater accuracy and insight – *e.g.*, into the facts that for n^{th} sub-harmonic injection locking, the number of locks is a multiple of n, and that these n locks are equally spaced in phase with gaps of $\frac{2\pi}{n}$. A pleasing feature of our graphical approach is that it does not involve many iterations (even though IL is a fundamentally nonlinear problem), but finds solutions in exactly one pass. Our technique for SHIL also subsumes FHIL as a special case.

The **MATLAB**™ tool implementing our mixed computational-analytical approach allows us to analyse SHIL in practical LC oscillator topologies. We present detailed results on two types of LC oscillators: a cross-coupled differential pair topology favoured in RFICs, and a tunnel diode based topology popular in UHF applications. We provide graphical depictions of locking, predicting the amplitudes/phases of locks and the lower/upper limits of lock ranges. We validate our predictions against brute force simulation, demonstrating essentially perfect matches. Our MATLAB-based tool provides these predictions 1-2 orders of magnitude faster than SPICE-level simulation (using NGSPICE [26], implemented in C/C++).

The remainder of the paper is organized as follows. In §II, we start by reviewing the describing function approach for predicting natural oscillations in LC oscillators. In §III, we present the graphical procedure noted above for SHIL. In §IV we use our theory and tool to analyse a cross-coupled BJT differential pair oscillator and a tunnel diode oscillator, validating our results using SPICE-level simulations.

II. Background: Describing Function analysis

The describing function approach mentioned in §I, is used for solving systems of the kind depicted in Fig. 1a. Here L is a linear time-invariant system with a nonlinear feedback N present from its output to input. The transfer function L only depends on the input frequency ω, whereas the transfer function N depends, among other things, on the input amplitude, say, A, but not on the input frequency ω. There are methods (*e.g.*, based on describing functions) for finding if this system can exhibit stable oscillations, and for finding these periodic waveforms if it does (under some 'filtering' assumptions, as we will see soon). As will become clear shortly, the describing function approach splits up the closed loop at the output (marked V_{out}

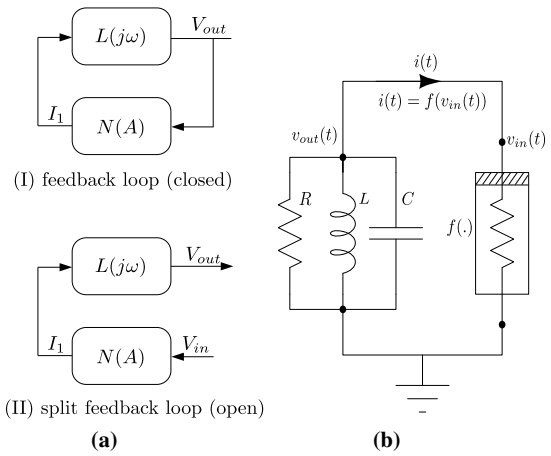

Fig. 1: (a) Linear system L with a nonlinear feedback N. (b) RLC circuit with negative resistance nonlinearity $f()$.

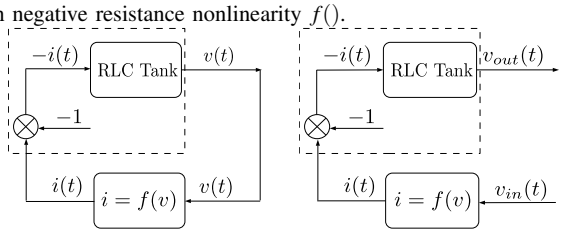

Fig. 2: (a) Circuit seen as a nonlinear feedback loop. (b) Nonlinear feedback loop with the feedback open for analysis.

in Fig. 1a.I) and tries to match the V_{out} and V_{in} signals (see Fig. 1a.II) so that the closed loop becomes consistent. Let us look at one such method, which is described in [4].

Fig. 1b depicts the LC oscillator circuit that we will be analyzing throughout this paper. Here $f()$ is the negative resistance element. Fig. 2a is an equivalent closed loop block diagram representation of the same circuit; the dashed box represents the linear part L of the circuit. To analyze the behaviour of this circuit, we 'cut open' the output feedback (see Fig. 2b) in the block diagram representation of the circuit (and not in the actual physical circuit), and look at the $v_{out}(t)$s generated by different $v_{in}(t)$s at the input. Finally, our aim is to match $v_{out}(t)$ to $v_{in}(t)$ so that this open loop can be closed back again for the circuit to become consistent.

For reasons to become clear later, lets start by considering a sinusoidal waveform at the input at some frequency ω_0, say $A\cos(\omega_0 t)$ $(= v_{in}(t))$. This input passes through the nonlinearity $f(.)$ to produce an output current $i(t) = f(v_{in}(t))$. Since, the input is periodic and $f(.)$ is memoryless, it can be easily shown that the output current $i(t)$ would be periodic too, with the same frequency ω_0. Thus, $i(t)$ can be written in a Fourier series representation, say,

$$i(t) = \sum_{k=-\infty}^{\infty} I_k(A) e^{jk\omega_0 t}. \qquad (1)$$

The I_ks are called the coefficients of the kth harmonic component of $i(t)$, and they only depend on the input's amplitude A and the nonlinearity $f(.)$. This current $i(t)$, after going through an inversion, passes through the LTI system determined by the RLC tank (see Fig. 6). For an RLC tank with a good enough Q factor, as can be seen from the amplitude characteristic of the transfer function, all harmonics other than those near the centre frequency ω_c are significantly attenuated, or in other words, filtered out by the RLC tank, while the one at the centre frequency is amplified by a factor of R and its phase is preserved, *i.e.*, phase change $= 0$. Thus, if we choose the frequency ω_0 of our input $v_{in}(t)$ to be $= \omega_c$, implying the frequency of $-i(t)$ to be ω_c, all the higher harmonic components of $-i(t)$ (the input to the RLC tank) will be filtered out and only the fundamental harmonic components ($k = \pm 1$) of $-i(t)$ will survive, scaled by a factor of R at its output corresponding to the peak of the transfer function. *Thus, our assumption of considering a purely sinusoidal waveform at the input is now justified.* Also, note that we don't really care about the higher harmonics present in $i(t)$ since they don't come into play at the output, which we are basically interested in (these higher harmonics in $i(t)$ make it highly distorted).

For nonlinearities $f(.)$ with a negative differential resistance[2] characteristic near the operating point, it can easily be shown[3] that $\angle I_1(A) = \pi$ $(\Rightarrow \angle I_{-1}(A) = \pi$, since $I_{-1} = \bar{I}_1)$, *i.e.*, $I_1(A)$ is a negative real number. Thus, $v_{out}(t) = R(-I_1(A)e^{j\omega_c t} - I_{-1}(A)e^{-j\omega_c t}) = -RI_1(e^{j\omega_c t} + e^{-j\omega_c t}) = -2RI_1\cos(\omega_c t)$, is in phase with $v_{in}(t) = A\cos(\omega_c t)$. At this point, if we wish to close back the cut loop, we will need $v_{out}(t) = v_{in}(t)$, *i.e.*,

$$A = -2RI_1(A) \;\Rightarrow\; T_f(A) \triangleq \frac{-RI_1(A)}{A/2} = 1. \qquad (2)$$

Such an A, satisfying (2), can be found out graphically by plotting $y = 1$ and $y = \frac{-RI_1(A)}{A/2}$ (versus A, of course) curves together and then reading off the A component of the intersection, if any, as shown in Fig. 3 (this figure is for a negative 'tanh' nonlinearity $f()$ and we will be using this nonlinearity for illustration purposes throughout §III while developing our new theory). [4] plots $y = A/2R$ and $y = -I_1(A)$ curves instead. Our choice of plotting (2) is influenced by two factors: (a) $T_f(A)$ is the transfer function[4] from the input phasor $A/2$ $(A\cos(\omega_c t) = A/2e^{j\omega_c t} + A/2e^{-j\omega_c t})$ to the output phasor $-RI_1(A)$ $(-2RI_1(A)\cos(\omega_c t) = -RI_1(A)e^{j\omega_c t} - RI_1(A)e^{-j\omega_c t})$, and, we will be using the graphical visualization provided by phasors later to our advantage; (b) we will be using the $T_f(A)$ formulation later for finding the stability properties of the solutions.

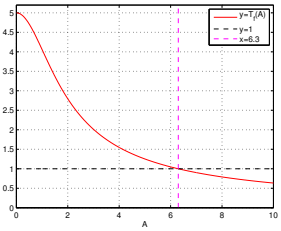

Fig. 3: Prediction of natural oscillations amplitude A for negative tanh LC oscillator.

III. MAIN THEORY

Here we outline our new theory for predicting SHIL, as we mentioned in §I. Due to space limitations many derivations are put in the appendix (§VI). We start by finding the stability of the natural oscillations (see §III-A) we just found in §II. Then we review the point of view taken in [4] for analyzing FHIL in negative-resistance LC oscillator circuits (see §III-B). Using a similar view point, we then elaborate how the describing function technique can be modified to understand SHIL (see §III-C) (as described in §I) in an intuitive yet precise and quantitative manner. We will see that small changes to the feedback loop Fig. 2b enable us to deal with IL.

A. Stability of Natural Oscillations

[4] doesn't comment on the stability of the solutions obtained through the graphical procedure (§II), but this is straightforward – the solution is stable iff the $y = \frac{-RI_1(A)}{A/2}$ curve cuts the $y = 1$ curve from above (see §VI-A1 for an explanation). Using this graphical procedure, we can see that the solution obtained in Fig. 3 is clearly a stable one.

B. Fundamental Harmonic Injection Locking (FHIL)

Before moving on to SHIL, we first review the basic point of view developed in [4] for analyzing the case of FHIL, so as to build foundation to provide a better understanding of the SHIL case.

After dealing with natural oscillations, [4] then goes on to analyze the same circuit but now in the presence of an external periodic disturbance (which we called the 'injection signal' in §I) at a frequency $\omega_i \approx \omega_c$. Our original circuit diagram and block diagram change in the manner as shown in Fig. 4a and Fig. 4b, respectively.

[2] later, by 'negative resistance' we will always mean a negative 'differential' resistance.

[3] in fact, for any general memoryless nonlinearity $f()$, $I_1(A)$ is a real number $\Rightarrow \angle I_1(A) = 0,\ or,\ \pi$.

[4] in a loose sense since it depends on the input amplitude A as well.

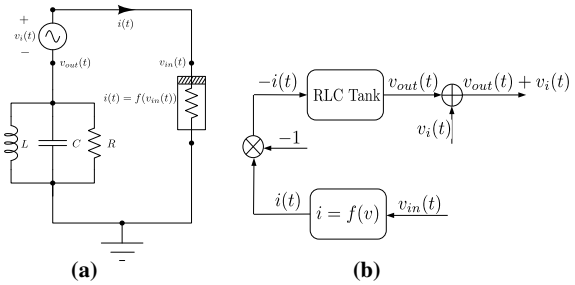

(a) (b)

Fig. 4: (a) Circuit diagram with added injection. (b) Split feedback loop with injection.

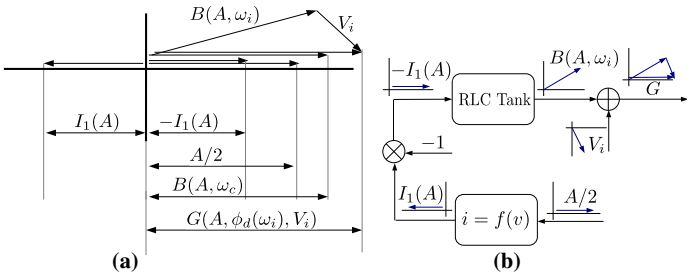

(a) (b)

Fig. 5: Phasor picture of the split feedback loop with injection present.

We are interested in the case where $\omega_i \approx \omega_c$, and the oscillator gets locked at the external signal frequency ω_i – thus, $v_{in}(t) = A\cos(\omega_i t)$ now. As shown in Fig. 4a and Fig. 4b, the input voltage waveform $v_{in}(t)$ passes through the nonlinearity block to give current $i(t)$, which then undergoes inversion, and gets filtered by the RLC tank to produce the output waveform $v_{out}(t)$. It is at this output that an injection signal $v_i(t)$ gets added. In terms of the phasor picture (see Fig. 5a), the input phasor $A/2$ (corresponding to the input waveform $v_{in}(t) = A\cos(\omega_i t)$) goes through the nonlinearity block $f()$ to produce a current $i(t)$ with fundamental harmonic component $= I_1(A)$. This current $i(t)$ then undergoes inversion, resulting in an inversion in its fundamental harmonic component as well, and further gets multiplied by the transfer function $H(j\omega)$ of the RLC tank resulting in $B(A,\omega_i) = -I_1(A)H(j\omega_i)$ at its output. It is at this stage that $v_i(t)$, also a sinusoid, with phasor domain signal V_i, gets added to $B(A,\omega_i)$ to produce the final output G. Some subtle points to note here. I_ks don't get affected by this change in the input frequency. Also, the higher harmonics of $-i(t)$ are still filtered out since $\omega_i \approx \omega_c$.

As we can see, this split feedback loop diagram is similar to the one described in §II, except for two major differences. Firstly, there is an additive injection signal $v_i(t)$ (or, phasor V_i) present at the output $v_{out}(t)$ (or, $B(A,\omega_i)$) of the split feedback loop, as can be clearly seen in the diagrams. Secondly, we are now operating at frequency ω_i – *i.e.*, the frequency of the injection signal, not at the centre frequency ω_c of the RLC tank as in §II. This is because here we are interested in analyzing the case where the oscillator has "forgotten" its natural oscillation frequency, and now runs at the injection signal frequency. Note that this follows directly from the definition of injection locking (§I).

These two differences cause the corresponding phasor picture to change in a subtle way (see Fig. 5a and Fig. 5b). Due to the change in operating frequency, the RLC tank no longer preserves the phase of its input fundamental at its output (the phase increases or decreases depending on whether $\omega_i < \omega_c$ or $\omega_i > \omega_c$, respectively; see Fig. 6). That is, the phase of $B(A,\omega_i)$ $(= \phi_d(\omega_i) = \angle H(j\omega_i))$ is non-zero. Note that this phase depends only on the operating frequency ω_i. Thus, the split loop, if now closed is clearly not consistent for any value of $A \neq 0$, *i.e.*, $B(A,\omega_i) \neq A, \quad \forall A \neq 0,\ \omega_i \neq \omega_c$.

Here comes the role of the first difference, *i.e.*, the additive injection signal: the injection signal just makes up for this vector/phasor difference and makes the loop, when closed, consistent. In terms of the phasor diagram, this can be translated into choosing V_i such that G equals A. (Earlier, while dealing with natural oscillations, no injection was needed to make the closed loop consistent. This was possible because $\angle B(A,\omega_c)$ was $= 0 = \angle A$.)

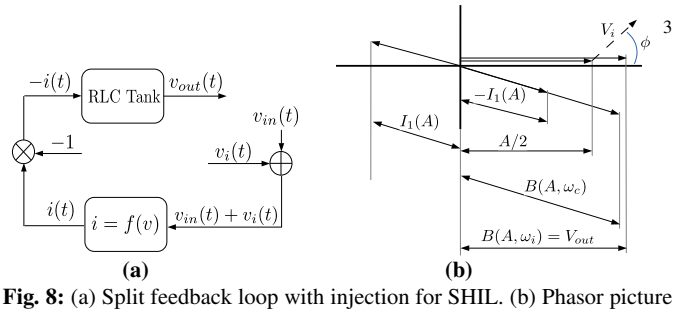

(a) (b)

Fig. 8: (a) Split feedback loop with injection for SHIL. (b) Phasor picture for SHIL.

Note that our upper system block (see Fig. 4b) is no longer linear now, but affine. Thus, the describing function theory in its original form for systems in Fig. 1a form can't be applied and needs modifications to analyze the important case of IL.

Using some of the ideas outlined in this subsection, we now move forwards to provide the theory for SHIL.

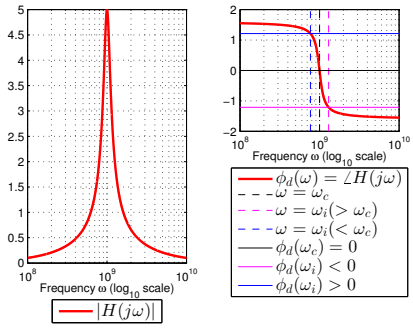

Fig. 6: RLC Tank transfer function.

C. Sub-harmonic Injection Locking (SHIL)

Here too, we consider an external injection signal present, but now we assume its frequency to be $n\omega_i$ instead, where $\omega_i \approx \omega_c$, and n is a natural number > 1 ($n = 1$ corresponds to FHIL case). This leads to a subtle difference compared to the FHIL case: at an operating frequency other than the centre frequency ω_c, the $v_i(t)$ signal can no longer be used to close the loop (or, restore consistency), since it is at a different frequency from the input $v_{in}(t)$ and output $v_{out}(t)$. Thus, a different mechanism is at play here. Note that due to the higher harmonic filtering assumption still valid, $v_{out}(t)$ is still a sinuosoid but $g(t) = v_{out}(t) + v_i(t)$ has both the fundamental and n^{th}-harmonic components present.

Thus, we now need to account for the n^{th}-harmonic component as well at the input $v_{in}(t)$, for consistency. Another point to note is that apart from the fundamental and n^{th}-harmonic components, no other harmonics are present in $g(t)$ or $v_{in}(t)$.

To account for the above changes, we do a small modification in Fig. 4b to get Fig. 8a, so that, in the light of the above discussion, $v_{in}(t)$ still remains a sinusoid $(= A\cos(\omega_i t))$. Since V_i can no longer be used to align V_{out} with $A/2$ directly, these two phasors should be aligned by default when the oscillator is under lock, if locking is still possible. The role of the n^{th}-harmonic component at the input to the nonlinearity $f()$ now immediately becomes clear – to provide appropriate phase shift in $-I_1$ (recall that it was $= 0$ in the FHIL case) so as to counter the phase shift produced by the RLC tank at the operating frequency ω_i. (Note that this viewpoint is general and also works for $n = 1$.)

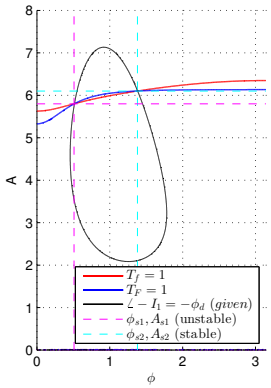

Fig. 7: Finding solutions for SHIL for a given V_i and ω_i.

Using the above ideas, it can be shown (§VI-B2) that the

$$T_f(A,V_i,\phi) = \frac{-RI_{1x}(A,V_i,\phi)}{A/2} = 1 \qquad (3)$$

$$\angle -I_1(A,V_i,\phi) = -\phi_d \qquad (4)$$

$$T_F(A,V_i,\phi,\phi_d) = \left|\frac{RI_1\cos(\phi_d)}{A/2}\right| = 1 \qquad (5)$$

solution should satisfy (3) and (4) (or equivalently, (5) and (4)), where I_{1x} is the cosine or x- component of phasor I_1. Now using (3) and (4) ((5) and (4)) let us first look at the simpler problem of finding the solutions given the operating frequency ω_i and the injection strength V_i. Note that for a given V_i and ω_i, T_f (T_F) and $\angle -I_1$ are 3D plots in variables A and ϕ. Let $C_{T_f,1}$ ($C_{T_F,1}$) be the cross-section of $z=T_f$ ($z=T_F$) surface with the $z=1$ plane. Similarly, let $C_{\angle -I_1,-\phi_d(\omega_i)}$ be the cross-section of the $z=\angle -I_1$ surface with the $z=-\phi_d(\omega_i)$ plane. Clearly, $C_{T_f,1}$ ($C_{T_F,1}$) is the set of all A,ϕ that satisfy (3) ((5)), and $C_{\angle -I_1,-\phi_d(\omega_i)}$ is the set of all A,ϕ that satisfy (4). Thus, the intersections of $C_{T_f,1}$ ($C_{T_F,1}$) and $C_{\angle -I_1,-\phi_d(\omega_i)}$ curves gives us our solutions (see Fig. 7). The stability of a solution is checked using the signs of T_F-1 and $\angle -I_1, \phi_d(\omega_i)+\phi_d$, and the relative slopes of $C_{T_F,1}$ and $C_{\angle -I_1,-\phi_d(\omega_i)}$ in the neighbourhood of the solution. Consider, for *e.g.*, (ϕ_{s2},A_{s2}). Around it, $\angle -I_1+\phi_d>0$ to the right of $C_{\angle -I_1,-\phi_d(\omega_i)}$, and <0 to the left of it. Also, $T_F<1$ below $C_{T_F,1}$, and >1 above it. For such a local picture, the solution is stable if the magnitude of the slope of $C_{\angle -I_1,-\phi_d(\omega_i)}$ is $>$ than that of $C_{T_F,1}$ (see §VI-B3). This condition holds and (ϕ_{s2},A_{s2}) is a stable solution. The local picture around (ϕ_{s1},A_{s1}) is different ($\angle -I_1+\phi_d$ is now <0 on the right and >0 on the left of $C_{\angle -I_1,-\phi_d(\omega_i)}$), and it can be shown using a similar logic that (ϕ_{s1},A_{s1}) is unstable.

Another interesting point to note here is that for any stable (unstable) solution (ϕ_s,A_s), there are n 'states' corresponding to it that are possible (see §VI-B4), namely: $(\phi_s+\frac{2\pi k}{n},A_s)$, $k=0,1,...,n-1$ (see Fig. 9).

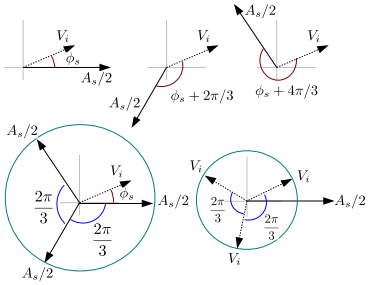

Fig. 9: Phasor picture depicting n states of n[th]-harmonic SHIL (for n=3).

Next, we look at the problem of finding the lock range given V_i (ω_i is unknown now). With changing ω_i, $C_{T_f,1}$ remains the same, but $C_{T_F,1}$ and $C_{\angle -I_1,-\phi_d(\omega_i)}$ change, since ϕ_d is a function of ω_i. Thus, we can cylindrically extend $C_{T_f,1}$ along the z-axis in both the directions and look for its intersection with the $z=\angle -I_1$ surface.

This intersection will be a curve and reading off the largest z-component (in terms of magnitude) on this curve that still leads to a stable lock gives us the maximum phase deviation, and thus the lock range. We depict this 3D procedure in 2D using isolines of the 3D surface $z=\angle -I_1$ for (a) ease in visualization, and, (b) examining the stability (see Fig. 10). We draw the isolines of $\angle -I_1$ and look for the maximum possible $|-\phi_d|$ visually (see Fig. 10) such that a stable lock is still possible. Stability of an intersection is checked in the same way as before. Invariance of $C_{T_f,1}$ makes this procedure computationally cheap, since the $C_{T_F,1}$ and $C_{\angle -I_1,-\phi_d(\omega_i)}$ curves have to be drawn only locally around the $C_{T_f,1}$ curve (even less than in Fig. 10). Fig. 10 is qualitatively similar to Fig. 7. Thus, if two solutions correspond to an isoline of $\angle -I_1$, the left one is unstable and the right one is stable $\Rightarrow$ at least one (exactly one in this case) stable solution is present till $-\phi_d=-0.295$, and no stable solution is present for higher $|-\phi_d|$ (no solution in this case). This value of $-\phi_d$ marks the boundary of the lock range.

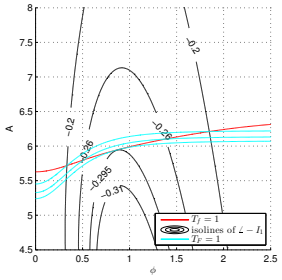

Fig. 10: Predicting SHIL lock range.

Two types/levels of speedup are possible compared to simulation: (a) While doing simulation, a 'binary search' needs to be done over different frequencies to find the lock range upto a certain accuracy. The same binary search needs to be done while using the prediction theory as well, if done in a graphical way (though it is more reliable since checking for a lock can sometimes be tricky while doing simulations). But this process can be automated (inside the code, by comparing the slopes as was pointed earlier). (b) Another is the time required to do one instance of simulation.

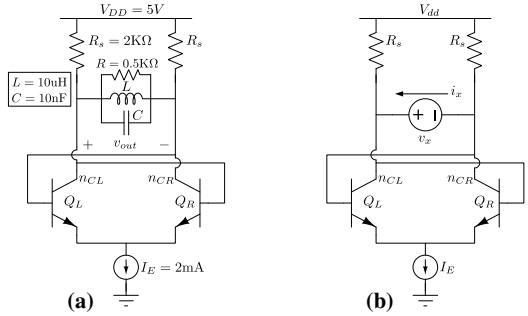

(a) **(b)**

Fig. 11: (a) Cross-coupled BJT differential pair oscillator. (b) Circuit used for finding the $i=f(v)$ curve for the diff-pair circuit Fig. 11a.

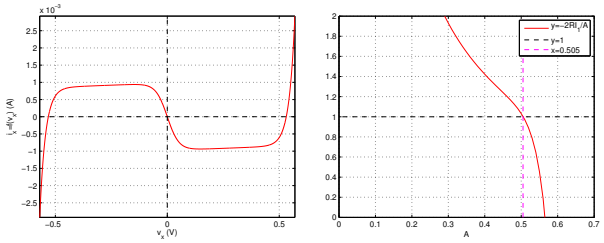

(a) **(b)**

Fig. 12: (a) Plot of the DC sweep, and hence the $i=f(v)$ curve, for the diff-pair. (b) Predicting the amplitude of steady state natural oscillations of diff-pair to be $A=0.505$V.

IV. ILLUSTRATION, RESULTS AND VALIDATION

In this section, we validate the theoretical predictions developed before in §III, by doing transient simulations on a cross-coupled BJT differential pair oscillator, and a tunnel diode oscillator.

A. Cross-coupled BJT Differential Pair Oscillator

Fig. 11a shows the schematic of the diff-pair oscillator circuit. The default NPN model in NGSPICE (with $I_s=10^{-12}$A) is used for the BJTs. The nodes n_{CL} and n_{CR} are the two terminals we are interested in, and the $i=f(v)$ relation is seen across these two terminals. The voltage difference between these nodes is marked as v_{out} in the circuit diagram. It is across these two nodes that we insert the RLC tank and expect the waveform v_{out} to be periodic.

Fig. 11b shows the schematic of the circuit used to run a DC sweep for extracting the $i=f(v)$ curve. Fig. 12a shows the extracted $i_x=f(v_x)$ curve (i_x and v_x are defined in Fig. 11b). Having obtained $f()$, we are now in a position to apply our prediction theory of §III.

1) Natural Oscillations: We start by predicting the presence and the amplitude of natural oscillations (see Fig. 12b), and validate it against transient simulation (see Fig. 13).

Fig. 13 shows the natural oscillations that emerge during the transient simulation of the diff-pair. As can be seen, after some initial transients, the circuit settles down in a periodic steady state. A close examination of these steady state oscillations show that the oscillation waveforms are sinusoids (see Fig. 13) with a frequency of 0.5033 MHz. This is, indeed, consistent with our assumption in §II that all higher harmonic components gets filtered out by the RLC tank, and the oscillation frequency is equal to the centre frequency of the tank.

2) SHIL: Next, we inspect 3[rd] SHIL for $|V_i|=0.03$V, say (Fig. 14). We don't plot the $T_F=1$ curves here for clarity since they almost overlap with the $T_f=1$ curve. Due to the same reasons as was noted for Fig. 10, in the case where an isoline of $\angle -I_1$ intersects $T_f=1$ curve twice, the solution to the right is the stable one. We note that A (and ϕ) decreases with increasing $|\omega_c-\omega_i|$ till a cut-off point is reached, after which a stable lock is not possible – giving us our lock range.

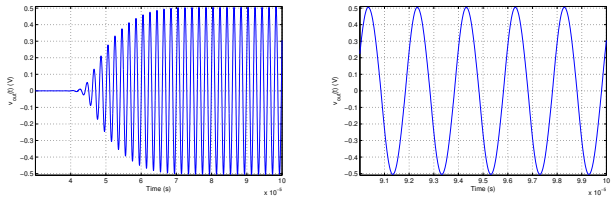

Fig. 13: Transient simulation of the diff-pair validating the predicted steady state natural oscillations amplitude of $A = 0.505$V.

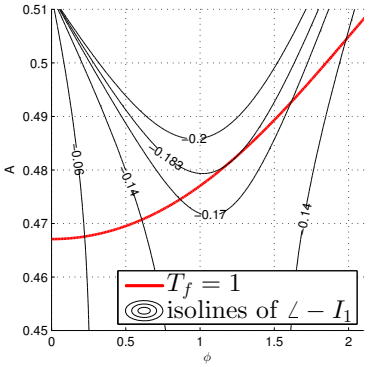

Fig. 14: Predicting the SHIL lock range of the diff-pair.

To facilitate state change, pulses of roughly 1.5us duration are given at time instances of 2ms and 4ms and all three states ($n = 3$ here) are observed (see Fig. 15). Note that the state change is seen with respect to the reference signal – a signal at $1/n^{\text{th}}$ of the injection signal frequency and phase locked with the injection signal.

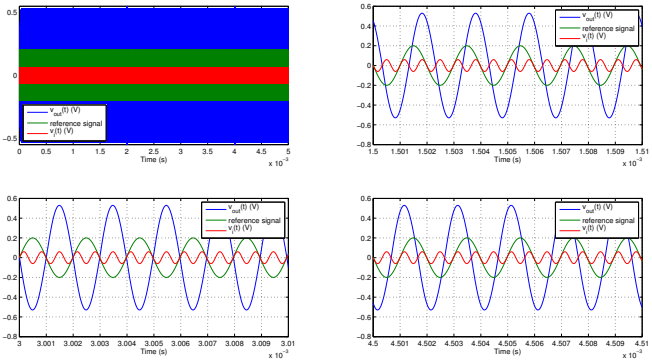

Fig. 15: SHIL states of the differential pair oscillator.

SHIL	lower lock limit	upper lock limit	lock range Δf
Simulation	1.4998 MHz	1.5174 MHz	0.0176 MHz
Prediction	1.501065 MHz	1.518735 MHz	0.01767 MHz

We see that the value of A for SHIL is lower than that for natural oscillations. Here, compared to simulation, a speedup of about 25 times is achieved.

B. Tunnel Diode Oscillator

Fig. 16a shows the schematic of a tunnel diode oscillator. Details about the model used for the tunnel diode can be found in §VI-C.

We proceed in the same order as the previous diff-pair example, and obtain the $i = f(v)$ curve first for the tunnel diode (Fig. 16b), for using it in our prediction theory of §III. The $i = f(v)$ immediately brings out the fact that the tunnel diode acts as a negative resistance for operating points near 0.25V (unlike 0V as in the diff-pair example). Thus, as is seen in Fig. 16a, we bias it around this operating point. This shifts the $i = f(v)$ curve to the left by a distance of 0.25V, bringing the negative resistance part above the origin.

1) Natural Oscillations: Fig. 16c predicts the presence of natural oscillations and its amplitude in the tunnel diode oscillator and Fig. 17

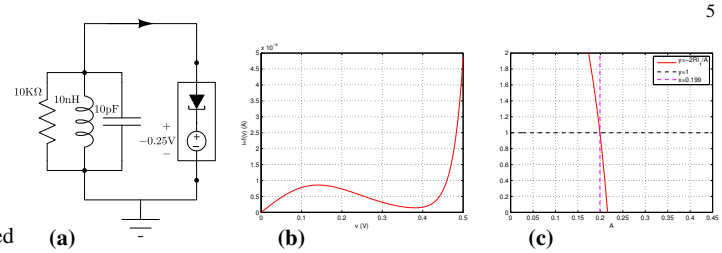

Fig. 16: (a) Tunnel diode oscillator. (b) Tunnel diode's $i = f(v)$ curve. (c) Predicting the amplitude of natural oscillations for the tunnel diode oscillator to be $A = 0.199$V.

is the transient simulation that validates the prediction. We observe that the steady state natural oscillations are sinusoidal again, with a frequency of 0.5033 GHz – consistent with the filtering assumption and centre frequency of the RLC tank.

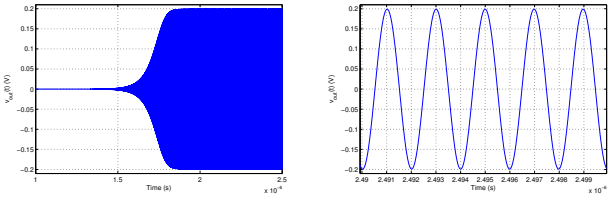

Fig. 17: Transient simulation of the tunnel diode validating the predicted steady state natural oscillations amplitude of $A = 0.199$V.

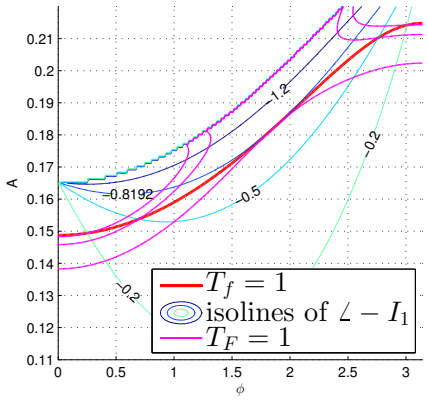

Fig. 18: Predicting the SHIL lock range of the tunnel diode oscillator.

2) SHIL: Next, we inspect 3rd SHIL for $|V_i| = 0.03$V, say (see Fig. 18). Here too, the qualitative nature of the plot (which defines the stability of the solutions) is the same as that of Fig. 14 and Fig. 10. Thus, A and ϕ decrease with increasing frequency deviation upto a cut-off point which marks the boundary of the lock range.

SHIL	lower lock limit	upper lock limit	lock range Δf
Simulation	1.507185 GHz	1.512293 GHz	0.005108 GHz
Prediction	1.507320 GHz	1.512429 GHz	0.005109 GHz

Now, we give pulses of 1ns duration at time instances of 2us and 4us to facilitate state change (see Fig. 19) and all three states ($n = 3$ here) are observed (states seen with respect to the reference signal, as before).

Here, again, the value of A for SHIL is lower than that for natural oscillations. For this example, compared to simulation, a speedup of about 50 times is achieved.

V. CONCLUSION

Here we provide a technique for analyzing SHIL in negative-resistance LC oscillators, that apart from being general and rigorous, is also the simplest and most insightful treatment of SHIL to date. Our procedure is developed in an elegant analytical way so that it can be viewed graphically thus providing intuition and much more design

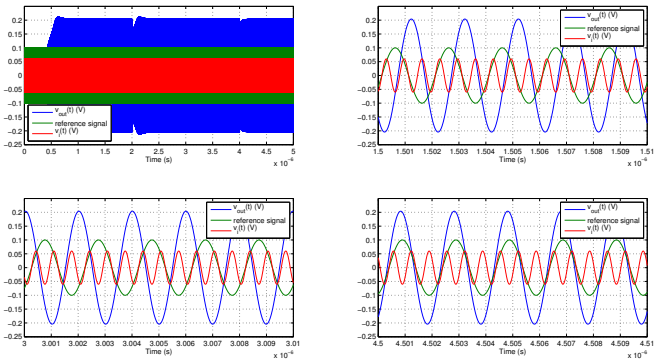

Fig. 19: SHIL states of the tunnel diode oscillator.

insights into SHIL compared to simulation. Also, all the solutions can be found and viewed graphically much faster than simulation. Our approach can deal with any type of nonlinearity in the circuit by resorting to computational approach, rather than assuming any specific form on the nonlinearity.

REFERENCES

[1] R. Adler. A study of locking phenomena in oscillators. 34:351–357, June 1946. Reprinted as [2].

[2] R. Adler. A study of locking phenomena in oscillators. *Proc. IEEE*, 61:1380–1385, 1973. Reprinted from [1].

[3] B. Razavi. A study of injection pulling and locking in oscillators. In *IEEE CICC 2003*, pages 305–312, October 2003.

[4] Y. Wan, X. Lai, and J. Roychowdhury. Understanding injection locking in negative-resistance lc oscillators intuitively using nonlinear feedback analysis. pages 729–732, 18-21 Sept. 2005.

[5] M. Armand. On the output spectrum of unlocked driven oscillators. 57:798–799, May 1969.

[6] S. Verma, H.R. Rategh, and T.H. Lee. A unified model for injection-locked frequency dividers. 38(6):1015–1027, Jun 2003.

[7] P. Kinget, R. Melville, D. Long and V. Gopinathan. An injection-locking scheme for precision quadrature generation. 37(7):845–851, July 2002.

[8] L. Goldberg, H.F. Taylor, J.F. Weller, and D.M. Bloom. Microwave signal generation with injection-locked laser diodes. 19(13):491–493, June 1983.

[9] S. Kobayashi and T. Kimura. Injection locking characteristics of an AlGaAs semiconductor laser. *IEEE J. Quantum Electron.*, 16:915–917, September 1980.

[10] P. Goyal, X. Lai and J. Roychowdhury. A Fast Methodology for First-Time-Correct Design of PLLs Using Nonlinear Phase-Domain VCO Macromodels. pages 291–296, January 2006.

[11] J.C. Leloup and A. Goldbeter. Toward a detailed computational model for the mammalian circadian clock. pages 7051–7056, June 2003.

[12] S. Agarwal and J. Roychowdhury. Efficient Multiscale Simulation of Circadian Rhythms Using Automated Phase Macromodelling Techniques. In *Proc. Pacific Symp. Biocomputing*, volume 13, pages 402–413, January 2008.

[13] A. Zarroug, P.S. Hall, and M. Cryan. Active antenna phase control using subharmonic locking. 31(11):842–843, 1995.

[14] C.H. Chien and G.C. Dalman. Subharmonically injected phase-locked IMPATT-oscillator experiments. 6(8):240–241, 1970.

[15] A.S. Daryoush, T. Berceli, R. Saedi, P.R. Herczfeld and A. Rosen. Theory of subharmonic synchronization of nonlinear oscillators. pages 735–738 vol.2, 1989.

[16] L. Gustafsson, K.I. Lundstrom and G.H.B. Hansson. Basic Properties of Subharmonic Injection Locking. 21(1):28–34, 1973.

[17] A. Neogy and J. Roychowdhury. Analysis and Design of Subharmonically Injection Locked Oscillators. Mar 2012.

[18] J. Lee and H. Wang. Study of Subharmonically Injection-Locked PLLs. 44(5):1539–1553, 2009.

[19] J. Lee, H. Wang, W-T. Chen and Y-P Lee. Subharmonically injection-locked PLLs for ultra-low-noise clock generation. pages 92–93,93a, 2009.

[20] Y. Kobayashi, S. Amakawa, M. Ishihara, and K. Masu. A low-phase-noise injection-locked differential ring-VCO with half-integral subharmonic locking in 0.18μm CMOS. In *Proc. ESSCIRC*, pages 440–443, 2009.

[21] S-W. Tam, E. Socher, A. Wong, Y. Wang, L.D. Vu and M-C F. Chang. Simultaneous sub-harmonic injection-locked mm-wave frequency generators for multi-band communications in CMOS. In *Proc. RFIC Symp.*, pages 131–134, 2008.

[22] S. Dal Toso, A. Bevilacqua, M. Tiebout, S. Marsili, C. Sandner, A. Gerosa and A. Neviani. UWB Fast-Hopping Frequency Generation Based on Sub-Harmonic Injection Locking. 43(12):2844–2852, 2008.

[23] A. Winfree. Biological Rhythms and the Behavior of Populations of Coupled Oscillators. 16:15–42, 1967.

[24] A. Demir, A. Mehrotra, and J. Roychowdhury. Phase Noise in Oscillators: a Unifying Theory and Numerical Methods for Characterization. 47:655–674, May 2000.

[25] A. Demir and J. Roychowdhury. A Reliable and Efficient Procedure for Oscillator PPV Computation, with Phase Noise Macromodelling Applications. 22(2):188–197, February 2003.

[26] NGSPICE – Open Source mixed mode, mixed level circuit simulator (based on Berkeley's Spice3f5). http://ngspice.sourceforge.net/.

VI. APPENDIX

Here we provide the proofs and derivations of the results used in the paper. §VI-A1 finds the stability of the natural oscillations found through the graphical procedure. §VI-B2 derives the procedure for finding the solutions for SHIL, §VI-B3 discusses their stability properties, and also comments on the general symmetry of the lock range. §VI-B4 justifies the existence of n states in n^{th}-SHIL. §VI-C provides the model of the tunnel diode used in §IV.

A. Natural Oscillations

1) Stability: Here we examine the stability of the natural oscillations. The solution is stable iff the $y = \frac{-RI_1(A)}{A/2}$ curve cuts the $y = 1$ curve from above. This can be seen by recalling that T_f is the open loop system's transfer function in the phasor domain. When the input amplitude A grows by a small positive amount δA, $T_f(A+\delta A) < 1$ and hence the system tries to reduce the input amplitude. Whereas, when the input amplitude falls by a positive amount, $T_f(A-\delta A) > 1$ and hence the system tries to increase the input amplitude. Thus, the system has a restoring effect overall making the solution stable. A similar argument can be used to show that the solution is unstable if $y = \frac{-RI_1(A)}{A/2}$ curve cuts $y = 1$ from below – hence the 'iff' part in the original statement.

B. SHIL derivations

1) Circle property: The following property will be helpful and used later to do the derivations for the SHIL case (see Fig. 20):

For a fixed input phasor, the output phasor of the RLC tank circuit sweeps a circle as the operating frequency is varied continuously. Also, the diameter of this circle is the output phasor when operating at the centre frequency. In other words, the locus of the head of the output phasor $B(A,\omega_i)$ is a circle with diameter as the phasor $B(A,\omega_c)$. In Fig. 20, we denote $B(A,\omega_c)$ by B, and $B(A,\omega_i)$ by B_o. M is the mid-point of OB and the centre of the circle.

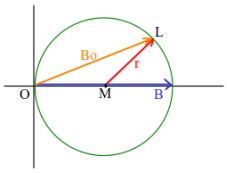

Fig. 20: Circle property of the RLC tank circuit.

Using the fact that the diameter of a circle subtends a right angle at the circumference (see Fig. 21), the output phasor $B(A,\omega_i)$ of the RLC tank at any given operating frequency ω_i can be easily found by projecting $B(A,\omega_c)$ along the $\phi_d(\omega_i)$ direction (*i.e.*, the direction that makes an angle of $\phi_d(\omega_i)$ from the horizontal).

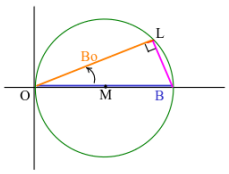

Fig. 21: Use of the circle property.

2) Finding the solutions: Here we derive the method used for finding solutions for the SHIL case.

See Fig. 8a and Fig. 8b. It is possible to write the Fourier series of $i(t) = f(A\cos(\omega_i t) + 2V_i\cos(n\omega_i t + \phi))$ since it remains periodic. But I_1 is no longer a function of A alone, and also depends on V_i and the phase difference ϕ between them.

For a lock to be possible, we need the fundamental harmonic components at the input and output to match, *i.e.*,

$$\begin{aligned} &A/2 = V_{out} = -I_1(A,V_i,\phi)H(j\omega_i) \\ &\Leftrightarrow \angle -I_1(A,V_i,\phi) + \angle H(j\omega_i) = 0, \\ &\textit{and},\ |I_1(A,V_i,\phi)||H(j\omega_i)| = |A/2| = A/2. \end{aligned} \tag{6}$$

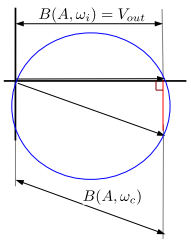

Fig. 22: Using circle property for SHIL.

The phase part of the above equation is,

$$\angle -I_1(A,V_i,\phi) + \angle H(j\omega_i) = \angle -I_1(A,V_i,\phi) + \phi_d = 0, \tag{7}$$

and the magnitude part is,

$$T_F = \left|\frac{I_1(A,V_i,\phi)R\cos(\phi_d)}{A/2}\right| = 1. \tag{8}$$

Simplifying using the circle property (see Fig. 22), we get,

$$\begin{aligned} &\angle -I_1(A,V_i,\phi) + \angle H(j\omega_i) = \angle -I_1(A,V_i,\phi) + \phi_d = 0 \\ &\Rightarrow |I_1(A,V_i,\phi)||H(j\omega_i)| = |I_1(A,V_i,\phi)||R\cos(\phi_d)| \\ &= R|-I_1(A,V_i,\phi)||\cos(\angle -I_1(A,V_i,\phi))| \\ &= R|-I_{1x}(A,V_i,\phi)| = A/2 \\ &\Rightarrow A/2 = V_{out} = -RI_{1x}(A,V_i,\phi), \end{aligned} \tag{9}$$

where I_{1x} is the cosine component of phasor I_1 and is thus independent of ω_i. Thus, the transfer function from the fundamental harmonic component of the input to the fundamental harmonic component of the output, when locked, is,

$$T_f(A,V_i,\phi) = \frac{-RI_{1x}(A,V_i,\phi)}{A/2}. \tag{10}$$

3) Stability: Here we analyze the stability of the solutions (A_s,ϕ_s) obtained for the SHIL case. We have two variables that can lead to instability of the lock, namely, A and ϕ.

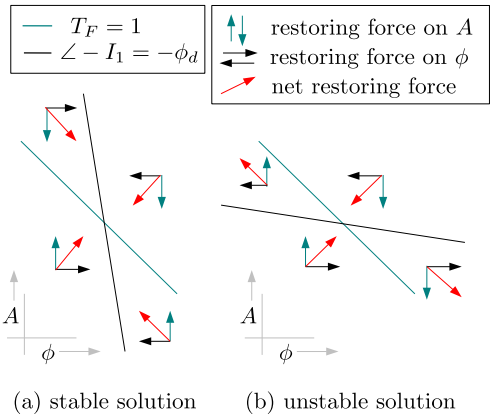

(a) stable solution (b) unstable solution

Fig. 23: Finding stability of solutions for SHIL.

In Fig. 23, we assume $T_F < 1$ above the $T_F = 1$ curve and > 1 below it. Also, $\angle -I_1 + \phi_d > 0$ to the right of $\angle -I_1 = -\phi_d$ curve and < 0 to the left of it (ϕ_d is fixed here). Other cases can be handled similarly. The vertical and horizontal vectors are the restoring forces in the A and ϕ components, respectively (note the directions, for *e.g.*, $\angle -I_1 + \phi_d > 0 \Rightarrow$ output phasor V_{out} rotates counterclockwise $\Rightarrow$ $A/2$ rotates counterclockwise $\Rightarrow$ phase difference between $A/2$ and V_i decreases $\Rightarrow$ ϕ decreases). The idea is to visualize the restoring force fields in the neighbourhood of the solution to find its stability. It can be easily shown, by visualizing the restoring force fields, that the solution is stable if the magnitude of the slope of the $\angle -I_1 = -\phi_d$ curve is $\geq$ the magnitude of the slope of the $T_F = 1$ curve; if $<$, and the slopes have the same sign, then the solution is unstable; if $<$, and the slopes have different signs then only looking at the directions of the force field is not sufficient for finding the local picture of the force field, but we won't get into the details here (in fact, thresholds can be found on the slopes at which the solution switches from a stable to an unstable one). For the examples encountered in this paper, seeing just the slopes is sufficient.

Another point to note is that if (ϕ_s, A_s) is a stable (unstable) solution, so is $(-\phi_s, A_s)$. This can be seen by substituting t by $-t$. Doing so results in conjugating the fundamental and n^{th} harmonic components everywhere, and thus flips the relative phase ϕ between the input and injection phasors. This will also require the RLC tank to cause a phase deviation of $-d$, if it was causing a phase deviation of d before. This is possible since RLC transfer function is even in amplification and odd in phase deviation around the centre frequency ω_c (see Fig. 6). Any perturbation that led to a restoring (diverging) effect before, will also do so now since all the new phasors are conjugates of the old ones, and conjugation is nothing but reflection about the x-axis. It can be easily shown that stability is preserved under reflections. This proves that the lock range is iso-directional about ω_c with respect to phase deviation, and thus is of the form $(\omega_c/p, p\omega_c)$, for some $p > 1$. This also justifies our plotting of the SHIL graphs only in the $0 \leq \phi \leq \pi$ range.

4) Existence of n states: Here we justify the existence of n states in n$^{\text{th}}$-SHIL. We start by showing that if (ϕ_s, A_s) is a stable (unstable) solution, so is $(\phi_s + \frac{2\pi}{n}, A_s)$. This can be seen by substituting t by $t + \frac{2\pi}{n\omega_i}$. By doing so, the n^{th} harmonic phasor remains unchanged (since $(n\omega_i(t + \frac{2\pi}{n\omega_i})) = (n\omega_i t + 2\pi)$), but the fundamental harmonic phasor everywhere gets rotated counterclockwise by $\frac{2\pi}{n}$ (since $(\omega_i(t + \frac{2\pi}{n\omega_i})) = (\omega_i t + \frac{2\pi}{n})$, I_1 changes to $I_1 e^{j\frac{2\pi}{n}}$ upon this time substitution). It can be easily shown that stability is preserved under translations in phase.

C. Tunnel Diode Equations

Here we provide the model for the tunnel diode that we used in §IV. The current I_{td} through the tunnel diode is given by,

$$I_{td} = I_{tunnel} + I_{diode}, \tag{11}$$

where I_{diode} is the p-n junction current given by,

$$I_{diode} = I_s(e^{\frac{v}{\eta V_{th}}} - 1), \tag{12}$$

and I_{tunnel} is the tunnel current given by,

$$I_{tunnel} = \frac{v}{R_0} e^{-(\frac{v}{V_0})^m}. \tag{13}$$

Here, I_s is the saturation current ($= 10^{-12}$A), η the ideality factor ($= 1$), V_{th} the threshold voltage ($= 0.025$V), typically $1 \leq m \leq 3$ ($= 2$) and $0.1 \leq V_0 \leq 0.5$ ($= 0.2$V), and R_0 is the resistance of the tunnel diode in the ohmic region ($= 1000\Omega$).